Yang, L., Gómez García, R., Muñoz Ferreras, J.M. & Zhang, R. 2020, "Input-reflectionless low-pass filter on multilayered diplexer-based topology", IEEE Microwave and Wireless Components Letters, vol. 30, no. 10, pp. 945-948

Available at http://dx.doi.org/10.1109/LMWC.2020.3017252

Input-Reflectionless Low-Pass Filter on Multilayered Diplexer-Based Topology

Li Yang, *Member, IEEE*, Roberto Gómez-García, *Senior Member, IEEE*, José-María Muñoz-Ferreras, *Member, IEEE*, and Runqi Zhang, *Member, IEEE*

***Abstract*—A class of input-reflectionless low-pass filter (LPF) using a multilayered diplexer-based architecture is presented. It consists of two signal-transmission parts: (i) a reflective-type LPF network built with an open-ended microstrip resonator and a shunt microstrip section, and (ii) a resistively-terminated wide-band microstrip-to-microstrip vertical transition. Thus, based on the in-band transmission poles of the wideband transition at which the RF-input-signal energy not transmitted by the LPF part is dissipated by the terminating 50-Ω resistor, a higher-selectivity LPF response with broadband reflectionless behavior is attained. To further increase the stopband bandwidth, as well as the attenuation levels and cut-off-slope sharpness, in-series-cascaded multi-LPF-unit designs are engineered. The main RF operational principles and theoretical design examples of the proposed input-reflectionless LPF approach are detailed. Moreover, for practical-validation purposes, a two-layered two-LPF-unit microstrip prototype with extended stopband and broadband input-reflectionless characteristics is designed, fabricated, and tested.**

***Index Terms*—Absorptive filter, diplexer-based circuit, input-reflectionless filter, low-pass filter (LPF), microstrip filter, multilayered circuit, vertical transition, wideband filter.**

I. Introduction

TO ELIMINATE the harmful effects of undesired RF input-signal power reflections in order to assure the robust operation of preceding microwave active circuits, RF absorptive/reflectionless filters are attracting a large interest in practical designs [1]. When compared to traditional reflective-type filters, the non-transmitted RF-input-signal energy at the stopband regions is expected to be fully dissipated inside the absorptive filter instead of being reflected back to the source [2]. Thus, a variety of reflectionless filtering components based on different design methods have been recently proposed, such as low-pass filters (LPFs), single-/multi-passband filters, filtering power dividers, and diplexers [3]–[15]. Regarding reflectionless LPFs, most of the experimental prototypes developed in [3]–[6], [11], and [12] are mainly designed with lumped-element networks and suffer from one or several of the following drawbacks: (i) large in-band power-insertion-loss levels, (ii) lack of multiple stopband power transmission poles in the absorptive-circuit part to attain a broadband reflectionless behavior, (iii) difficult scaling to higher frequency ranges, and (iv) high sensitivity to deviations in the lumped-element component values.

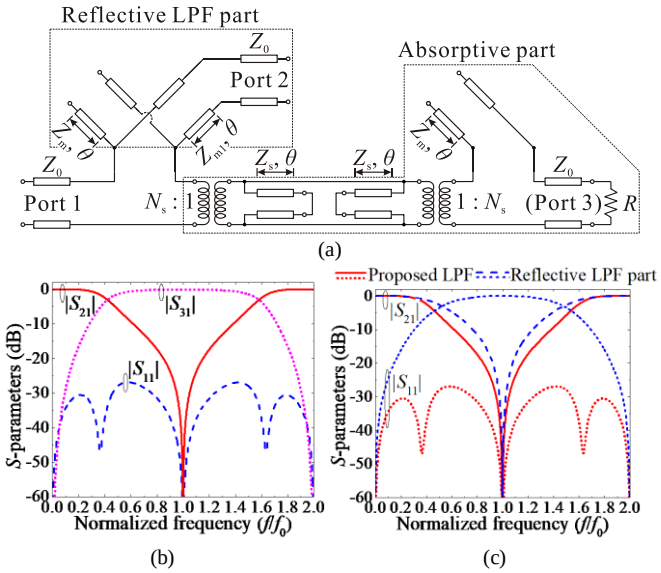

Fig. 1. Proposed input-reflectionless LPF. (a) Diplexer-based equivalent circuit using the resistively-terminated wideband microstrip-to-microstrip vertical transition in [16] when Z_m = 31.7 Ω, Z_s = 91.3 Ω, Z_{m1} = 78.1 Ω, N_s = 1, and R = 50 Ω. (b) Theoretical power transmission ($|S_{21}|$ and $|S_{31}|$) and input-reflection ($|S_{11}|$) responses of the diplexer-based network without the R resistor at port 3. (c) Theoretical $|S_{21}|$ and $|S_{11}|$ of the input-reflectionless LPF.

This letter presents input-reflectionless diplexer-based LPFs and their application to realize multi-LPF-unit designs with extended absorptive-stopband bandwidth and/or attenuation levels. The equivalent circuit of the engineered multilayered absorptive LPF is derived from the reflectionless wideband bandpass filters discussed in [15]. To the best of the authors' knowledge, this is the first time that two-layered microstrip-to-microstrip vertical transitions are applied to the development of absorptive/reflectionless LPFs. The theoretical foundations and RF operational principles of the proposed diplexer-based input-reflectionless LPF architecture are detailed. Furthermore, for practical-validation purposes, a microstrip two-LPF-unit prototype with stopband attenuation above 18.5 dB from 3.06 GHz to 14.3 GHz and input-power-matching levels higher than 10 dB from DC to 11.9 GHz is manufactured and characterized.

Manuscript received May 8, 2020; revised July 14, 2020 and August 10, 2020; accepted August 14, 2020. This work was supported in part by the Spanish Ministry of Economy, Industry, and Competitiveness (State Research Agency) under Project TEC2017-82398-R and in part by the GOT ENERGY TALENT (GET) fellowship programme co-funded by the EU as part of the H2020-MSCA-COFUND programme (Grant Agreement number 754382) . (*Corresponding authors: Li Yang; Roberto Gómez-García*.)

L. Yang, R. Gómez-García, and J.-M. Muñoz-Ferreras are with the Department of Signal Theory and Communications, University of Alcalá, Polytechnic School, Alcalá de Henares 28871, Madrid, Spain (e-mails: li.yang@uah.es; roberto.gomez.garcia@ieee.org; jm.munoz@uah.es).

Runqi Zhang is with the Akoustis, Inc., Huntersville, NC 28078 USA (e-mail: rzhang1@e.ntu.edu.sg).

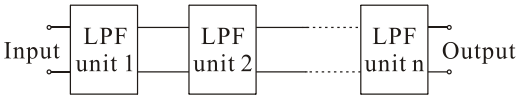

Fig. 2. Block diagram of the proposed extended-stopband input-reflectionless multi-LPF-unit network based on the in-series cascade of n LPF units as in Fig. 1(a) for Z_m = 31.7 Ω, Z_s = 91.3 Ω, Z_{m1} = 78.1 Ω, N_s = 1, and R = 50 Ω.

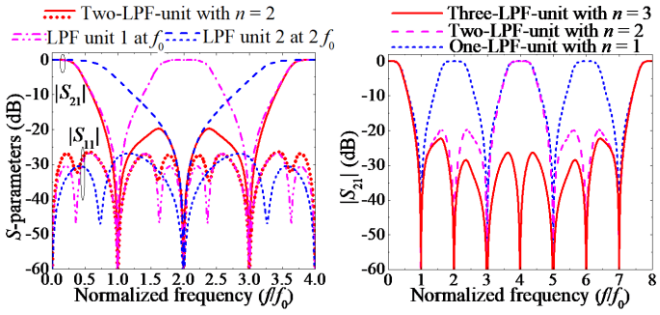

(a) (b)

Fig. 3. Theoretical power transmission ($|S_{21}|$) and input-reflection ($|S_{11}|$) responses of the proposed extended-stopband input-reflectionless multi-LPF-unit network. (a) Two-LPF-unit design with transmission-zero frequencies at f_0 and $2f_0$ for its building LPF units. (b) Multi-LPF-unit designs for n = 1, 2, 3.

II. Theory, Analysis, and Design

A. Diplexer-Based LPF Network

Fig. 1(a) depicts the equivalent circuit of the proposed input-reflectionless LPF. As shown, it is composed of two signal-transmission parts: (i) a reflective-type single-pole LPF shaped by an open-ended stub and a shunt transmission-line section and (ii) a wideband microstrip-to-microstrip vertical transition as in [16] terminated by a resistor at the output port (port 3) to dissipate the RF-input-signal energy not transmitted by the LPF part at its stopband range. Here, the open-ended stubs, the short-ended stubs, and the transmission-line section are set with the same electrical length θ—quarter-wavelength-long at f_0 as the stopband transmission-zero frequency of the reflective-type LPF—but different line impedances (Z_m, Z_s, and Z_{m1}). Z_0 is the 50-Ω port impedance and R is the resistance of the terminating resistor. Due to the existing end effect on the impedance variation of the slotline resonator in practice, two transformers with turns ratios of N_s are employed to account for it [16].

The operational principle of the devised LPF, initially assumed to be lossless with N_s = 1, is next detailed. By removing the terminating resistor at port 3, the wideband $2f_0$-frequency-periodic bandpass-type response of the vertical transition (with the specified in-band ripple factor of 0.002 dB and phase of 53.785° at the lower cut-off frequency of $0.598f_0$ or Z_m = 31.7 Ω and Z_s = 91.3 Ω [16]) is firstly calculated with transmission zeros occurring at 0, $2f_0$, …, $2Nf_0$ and transmission poles at f_0, $3f_0$, …, $(2N+1)f_0$ (N is a natural index). Note that two additional sets of transmission poles around f_0, $3f_0$, …, $(2N+1)f_0$ are generated when $z_m z_s > 1$ (z_m and z_s are the normalized-to-Z_0 line impedances). Thus, the reflective-type first-order LPF part with its first transmission zero at f_0 is designed. Meanwhile, Z_{m1} = 78.1 Ω is properly selected to maintain the power matching level $|S_{11}| \leq$ -20dB within the frequency range [0, $2f_0$) [15]. With these impedance values, the theoretical $2f_0$-frequency-periodic frequency responses of the diplexer network are obtained within the frequency range [0, $2f_0$), as shown in Fig. 1(b). In this manner, as the terminating resistor R = 50 Ω nearly consumes the non-transmitted RF-input-signal energy in the stopband range of the reflective-LPF part (full dissipation at f_0, $3f_0$, …, $(2N+1)f_0$) and owing to three in-band transmission poles of the wideband transition within [0, $2f_0$), both a high-selectivity lowpass-filtering-type transmission response and input-power-matching levels above 25 dB in a broad band are attained for the devised LPF, as proven in Fig. 1(c). Furthermore, the cut-off frequency of this absorptive LPF is increased for higher values of Z_m and/or lower values of Z_s, just in an opposite trend as the passband bandwidth of its wideband-vertical-transition part as discussed in [16].

B. Multi-LPF-Unit Designs with Extended Stopband

To realize an input-reflectionless low-pass filtering response with extended upper stopband, multiple LPF units as the one in Fig. 1 with spectrally-adjacent attenuated bands can be in-series cascaded as in [17], as shown in Fig. 2. Specifically, the in-series-cascaded LPF units of this multi-LPF-unit approach are designed with θ = 90° at different frequencies of their first transmission zero—i.e., f_0, $2f_0$, $4f_0$, …, $2^{n-1}f_0$, respectively. In this manner, the spectral locations of the out-of-band transmission zeros within its first attenuated band of the overall $2^n f_0$-frequency-periodic multi-LPF-unit network realized with n in-series-cascaded LPF units are f_0, $2f_0$, $3f_0$, …, $(2^n-1)f_0$.

From the above, it is derived that the first stopband of the input-reflectionless multi-LPF-unit network in Fig. 2 can be extended beyond $(2^n-1)f_0$, which is its upper out-of-band transmission-zero frequency. This is due to the joint action of the transmission zeros of its n building in-series-cascaded first-order LPF units. For illustration purposes, the theoretical power transmission and reflection responses of a two-LPF-unit example (i.e., n = 2 so that it is $4f_0$-frequency-periodic) and its constituent LPF units with transmission zeros at f_0 and $2f_0$ are drawn in Fig. 3. As shown in Fig. 3(a), based on the predicted transmission zeros, a stopband with attenuation levels above 20 dB up to more than $3f_0$ for the proposed two-LPF-unit network is obtained. Also, owing to the input-absorptive property of the proposed LPF, the input-reflectionless response of the overall two-LPF-unit circuit remains almost the same when compared to the one of the LPF unit 1. Fig. 3(b) compares the out-of-band responses of the multi-LPF-unit networks designed with n = 1, 2, and 3, respectively. As shown, the first upper stopband of the $8f_0$-frequency-periodic three-LPF-unit circuit can be extended beyond $7f_0$, which verifies the devised design strategy in Fig. 2.

III. Implementation and Discussion

To validate the experimental viability of the proposed input-reflectionless LPF based on a two-layered diplexer-type structure, a two-LPF-unit circuit with extended stopband up to above $3f_0$ (f_0 = 4 GHz) as in Section II.B has been designed, manufactured, and tested. The Roger's 4003C substrate with relative dielectric constant ε_r = 3.55, dielectric thickness h = 0.508 mm, metal thickness t = 35μm, and dielectric loss tangent $\tan(\delta_D)$ = 0.0027 is employed. Fig. 4 depicts the layout as well as the side-view structure of the conceived two-LPF-unit prototype, in which the open-ended stubs, the short-ended stubs, and the cascaded transmission-line sections in Fig. 1 are respectively realized as open-ended microstrip resonators,

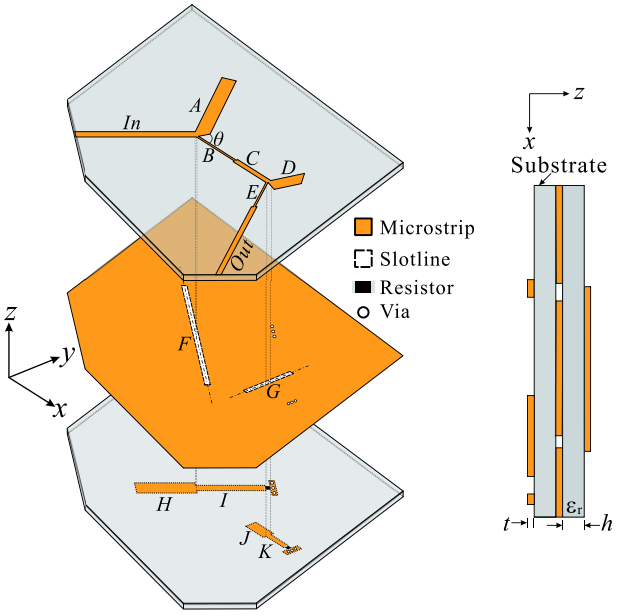

Fig. 4. Layout and side-view structure of the devised input-reflectionless two-LPF-unit prototype using two in-series-cascaded LPF units with different transmission-zero frequencies at 4 GHz and 8 GHz (L_{In} = 40, L_{Out} = 15, L_A = 8.44, L_B = 9.9, L_C = 7, L_D = 3.15, L_E = 4.45, L_F = 24.4, L_G = 12.4, L_H = 9.7, L_I = 6, L_J = 3.88, L_K =4, W_{In} = W_{Out} = W_C = W_I = W_K = 1.1, W_A = W_D = W_H = W_J = 2.6, W_B = W_E = 0.43, W_F = 0.5, W_G = 0.38, h = 0.508, t = 0.035 (unit: mm) and θ = 120°).

slotline resonators, and cascaded microstrip-line sections. As described in Section II.B, the in-series-cascaded LPF units of this devised two-LPF-unit prototype are initially designed with Z_m = 31.7 Ω, Z_s = 91.3 Ω, Z_{m1} = 78.1 Ω, and N_s = 1, but different transmission-zero frequencies at 4 GHz (f_0) and 8 GHz ($2f_0$). Nevertheless, due to the previously-mentioned end effect on the impedance variation of the slotline resonators in electromagnetic (EM) simulation, the impedance values of the Z_s parameters for the two employed LPF units are properly modified with Z_{s_1} = 109.03 Ω and Z_{s_2} = 116.61 Ω to make the EM-simulated responses fairly meet the theoretical ones. In this manner, the turns ratios of the employed transformers for these two LPF units are determined as N_{s_1} = 0.914 and N_{s_2} = 0.885 [16]. Moreover, two 50-Ω surface-mounted-device resistors with practically-measured resistances of 51.2 Ω and 51.6 Ω are soldered on the bottom layer. On the other hand, in order to avoid the coupling effect coming from the slotlines and the top-layer microstrip lines on the stopband power matching levels, the physical lengths of the 50-Ω microstrip lines connected with the resistors were carefully adjusted in the design process.

The theoretical, EM-simulated, and measured results of the manufactured two-LPF-unit prototype are depicted in Fig. 5(a). As shown, apart from some minor deviations observed in the upper spectral region of the measured input-power-reflection parameter that are mainly attributed to the frequency-dispersive nature of the substrate, the discontinuous effect of the SMA connectors, the influence of the packaging of the SMD resistors at high frequencies, and fabrication tolerances, a reasonably-close agreement among these frequency responses is obtained. The main performance metrics of the measured circuit are as follows: 1-dB bandwidth from DC to 1.31 GHz, first transmission-zero frequency at 3.97 GHz, 3-dB cut-off frequency of 1.73 GHz, stopband attenuation better than 18.5

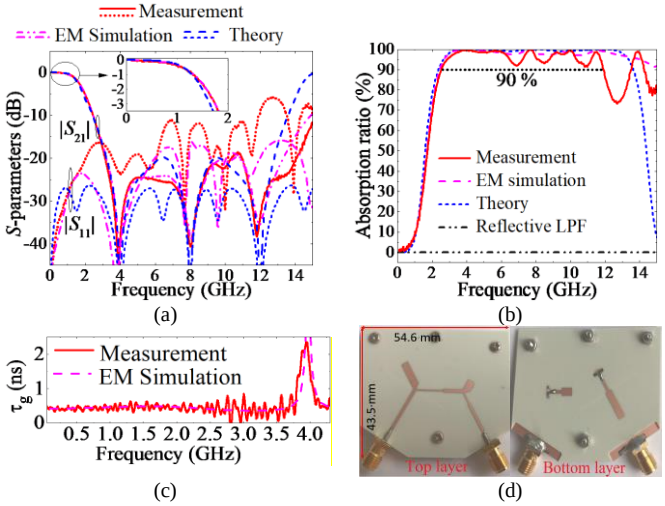

Fig. 5. Manufactured input-reflectionless two-LPF-unit microstrip prototype with layout in Fig. 4. (a) Theoretical, EM-simulated, and measured power transmission ($|S_{21}|$) and input-reflection ($|S_{11}|$) responses. (b) Simulated and measured input-power-absorption ratios (i.e., $100\times(1-|S_{21}|^2-|S_{11}|^2$ (%)). (c) Simulated and measured in-band group-delay (τ_g) responses. (d) Photographs of the assembled LPF prototype with size of 54.6×43.5 mm^2 or $0.52\lambda_g\times0.42\lambda_g$, where λ_g is the effective guided wavelength at the measured cut-off frequency.

TABLE I
COMPARISON WITH OTHER PRIOR-ART INPUT-REFLECTIONLESS LPFS

Ref.	1-dB BW (GHz)	RR(GHz) /RL (dB)	SS (GHz)	DT
[3]	DC–0.1	DC–1/≥ 12	0.3–1 (53 dB)	LE
[4] LPF in Fig. 20	DC–0.7	DC–5/≥ 16	1.3–5 (18 dB)	MMIC
[11] LPF in Fig. 17	DC–0.008	DC–0.08/ ≥ 18	0.01–0.08 (14 dB)	LE
This Work	DC–1.31	DC–11.86/ ≥ 11.21	3.06–14.3 (18.5 dB)	MS

BW: bandwidth; RR: reflectionless range; RL: return loss; SS: stopband suppression; DT: design technology; LE: lumped element; MMIC: monolithic microwave integrated circuit; MS: microstrip.

dB from 3.06 GHz to 14.3 GHz, and input-power- matching levels above 11.21 dB from DC to 11.86 GHz. Figure 5(b) plots the simulated and measured power-absorption ratios of this LPF. Compared to its reflective-type LPF part, an out-of-band power-absorption ratio above 90% for this LPF prototype is measured from 2.47 GHz to 11.95 GHz (i.e., 7.24 times the 1-dB bandwidth), which means a broad-band input-reflectionless property. The measured maximum in-band group-delay variation is 0.21 ns as depicted in Fig. 5(c), and Fig. 5(d) shows the top- and bottom-layer photographs of this assembled LPF prototype. Furthermore, a detailed comparison between the developed input-absorptive LPF prototype of this work and other prior-art reflectionless LPFs is given in Table I.

IV. CONCLUSION

A class of two-layered input-reflectionless diplexer-based LPF is reported in this letter. By using a resistively-terminated wideband microstrip vertical transition by the first time for this application, an input-reflectionless response for the conceived LPF device is realized. The RF operational foundations and theoretical examples of this input-reflectionless LPF design approach have been shown and experimentally verified with the development and characterization of a two-LPF-unit microstrip prototype with extended reflectionless stopband.

REFERENCES

[1] Mini-Circuits, Brooklyn, NY., "Reflectionless filters improve linearity and dynamic range," *Microw. J.*, vol. 58, no. 8, pp. 42–50, Aug. 2015.

[2] M. A. Morgan, "Think outside the band: Design and miniaturization of absorptive filters," *IEEE Microw. Mag.*, vol. 19, no. 7, pp. 54–62, Nov. 2018.

[3] M. A. Morgan and T. A. Boyd, "Theoretical and experimental study of a new class of reflectionless filter," *IEEE Trans. Microw. Theory Techn.*, vol. 59, no. 5, pp. 1214–1221, May 2011.

[4] M. A. Morgan and T. A. Boyd, "Reflectionless filter structures," *IEEE Trans. Microw. Theory Techn.*, vol. 63, no. 4, pp. 1263–1271, Apr. 2015.

[5] T.-H. Lee, B. Lee, and J. Lee, "First-order reflectionless lumped-element lowpass filter (LPF) and bandpass filter (BPF) design," in *Proc. IEEE MTT-S Int. Microw. Symp*, May 2016, pp. 1–4.

[6] M. Khalaj-Amirhosseini and M.-M. Taskhiri, "Twofold reflectionless filters of inverse-Chebyshev response with arbitrary attenuation," *IEEE Trans. Microw. Theory Techn.*, vol. 65, no. 11, pp. 4616–4620, Nov. 2017.

[7] D. Psychogiou and R. Gómez-García, "Reflectionless adaptive RF filters: Bandpass, bandstop, and cascade designs," *IEEE Trans. Microw. Theory Techn.*, vol. 65, no. 11, pp. 4593–4605, Nov. 2017.

[8] R. Gómez-García, J.-M. Muñoz-Ferreras, W. Feng, and D. Psychogiou, "Balanced symmetrical quasi-reflectionless single- and dual-band bandpass planar filters," *IEEE Microw. Wireless Compon. Lett.*, vol. 28, no. 9, pp. 798–800, Sep. 2018.

[9] R. Gómez-García, J.-M. Muñoz-Ferreras, and D. Psychogiou, "Split-type input-reflectionless multiband filters," *IEEE Microw. Wireless Compon. Lett.*, vol. 28, no. 11, pp. 981–983, Nov. 2018.

[10] R. Gómez-García, J.-M. Muñoz-Ferreras, and D. Psychogiou, "Dual-behavior resonator-based fully-reconfigurable input-reflectionless bandpass filters," *IEEE Microw. Wireless Compon. Lett.*, vol. 29, no. 1, pp. 35–37, Jan. 2019.

[11] M. A. Morgan, W. M. Groves, and T. A. Boyd, "Reflectionless filter topologies supporting arbitrary low-pass ladder prototypes," *IEEE Trans. Circuits Syst. I, Reg. Papers*, vol. 66, no. 2, pp. 594–604, Feb. 2019.

[12] T.-H. Lee, B. Lee, Y.-S. Kim, K. Wu, and J. Lee, ''Higher order lumped element absorptive low-pass and bandpass filter structures," *IET Microw., Antennas Propag.*, vol. 13, no. 8, pp. 1166–1173, Jun. 2019.

[13] B. Lee, S. Nam, and J. Lee, "Filtering power divider with reflectionless response and wide isolation at output ports," *IEEE Trans. Microw. Theory Techn.*, vol. 67, no. 7, pp. 2684–2692, Jul. 2019.

[14] R. Gómez-García, J.-M. Muñoz-Ferreras, and D. Psychogiou, "High-order input-reflectionless bandpass/bandstop filters and multiplexers," *IEEE Trans. Microw. Theory Techn.*, vol. 67, no. 9, pp. 3683–3695, Sep. 2019.

[15] L. Yang, R. Gómez-García, J.-M. Muñoz-Ferreras, R. Zhang, D. Peroulis, and L. Zhu, "Multilayered reflectionless wideband bandpass filters with shunt/in-series resistively terminated microstrip lines," *IEEE Trans. Microw. Theory Techn.*, vol. 68, no. 3, pp. 877–893, Mar. 2020.

[16] L. Yang, L. Zhu, W.-W. Choi, and K.-W. Tam, "Analysis and design of wideband microstrip-to-microstrip equal ripple vertical transitions and their application to bandpass filters," *IEEE Trans. Microw. Theory Techn.*, vol. 65, no. 8, pp. 2866–2877, Aug. 2017.

[17] R. Gómez-García, M. A. Sánchez-Soriano, M. Sánchez-Renedo, G. Torregrosa-Penalva, and E. Bronchalo, "Low-pass and bandpass filters with ultra-broad stopband bandwidth based on directional couplers," *IEEE Trans. Microw. Theory Tech.*, vol. 61, no. 12, pp. 4365–4375, Aug. 2013.